Modelling of electrokinetic phenomena for capture of PEGylated ribonuclease A in a microdevice with insulating structures

Marco A. Mata-Gomez,[a] Victor H. Perez-Gonzalez,[a]
Roberto C. Gallo-Villanueva, Jose Gonzalez-Valdez,
Marco Rito-Palomares, and Sergio O. Martinez-Chapa[b]
School of Engineering and Sciences, Tecnologico de Monterrey, Ave. Eugenio Garza Sada 2501 Sur, Monterrey, NL 64849, Mexico

(Received 27 February 2016; accepted 6 June 2016; published online 15 June 2016)

Synthesis of PEGylated proteins results in a mixture of protein-polyethylene glycol (PEG) conjugates and the unreacted native protein. From a ribonuclease A (RNase A) PEGylation reaction, mono-PEGylated RNase A (mono-PEG RNase A) has proven therapeutic effects against cancer, reason for which there is an interest in isolating it from the rest of the reaction products. Experimental trapping of PEGylated RNase A inside an electrokinetically driven microfluidic device has been previously demonstrated. Now, from a theoretical point of view, we have studied the electrokinetic phenomena involved in the dielectrophoretic streaming of the native RNase A protein and the trapping of the mono-PEG RNase A inside a microfluidic channel. To accomplish this, we used two 3D computational models, a sphere and an ellipse, adapted to each protein. The effect of temperature on parameters related to trapping was also studied. A temperature increase showed to rise the electric and thermal conductivities of the suspending solution, hindering dielectrophoretic trapping. In contrast, the dynamic viscosity of the suspending solution decreased as the temperature rose, favoring the dielectrophoretic manipulation of the proteins. Also, our models were able to predict the magnitude and direction of the velocity of both proteins indicating trapping for the PEGylated conjugate or no trapping for the native protein. In addition, a parametric sweep study revealed the effect of the protein zeta potential on the electrokinetic response of the protein. We believe this work will serve as a tool to improve the design of electrokinetically driven microfluidic channels for the separation and recovery of PEGylated proteins in one single step. *Published by AIP Publishing.* [http://dx.doi.org/10.1063/1.4954197]

I. INTRODUCTION

Mono-PEGylated ribonuclease A (mono-PEG-RNase A) is a modern type of therapeutic drug that has demonstrated therapeutic potential against cancer;[1,2] for this reason, it has gained increasing interest from the scientific and industrial communities. This protein is synthesized by covalently incorporating a poly-ethylene glycol (PEG) molecule into the native ribonuclease A (RNase A).[3] Moieties of PEG confer stability, higher solubility, and enhanced biological activity.[4,5] Nevertheless, PEGylation of the native protein yields two PEGylated conjugates that vary in the number of PEG molecules attached, and the unreacted protein. Therefore, it is important to develop new strategies to isolate the mono-PEG conjugate from the reaction mixture. Techniques, such as size exclusion chromatography (SEC) and hydrophobic interaction chromatography (HIC), are available to isolate this protein. However, these are time-consuming methods that require large volumes of buffer solutions and employ external pumps to carry the

[a]M. A. Mata-Gomez and V. H. Perez-Gonzalez contributed equally to this work.
[b]Author to whom correspondence should be addressed. Electronic mail: smart@itesm.mx

sample through the column and achieve separation. In contrast, microfluidic devices, which are portable and inexpensive, allow the manipulation of small sample amounts in shorter processing times. Additionally, depending on the design of the microfluidic device, the use of external pumps to drive sample motion can be avoided.[6]

It should be noted, however, that the method election to be used for the implementation of a separation strategy for a determined bioproduct depends on the amount of product required. In this sense, microfluidic systems and chromatographic strategies can complement each other. Microfluidic devices can be used, for instance, to monitor PEGylation reactions and to separate small amounts of high-value products, while chromatographic methods can be used to separate large amounts of products. Note that liquid-liquid separation strategies have also been explored.[7,8]

Electrokinetics (EKs) is a branch of physics that studies the induced motion of solids and fluids while in the presence of an electric field. EK phenomena have been successfully employed within microfluidic systems to manipulate the movement of a range of bioparticles, among which we can list yeast cells, virus, bacteria, microalgae, and DNA.[6,9–11] Hence, an alternative strategy that can be exploited for the manipulation of proteins is the use of EKs in microfluidic devices. Although microfluidic devices offer advantages like portability and reduced analysis time,[12] their use is still far from being a routine technique such as chromatography-based methods, especially for protein recovery.[13] Therefore, efforts in the design of devices that allow the separation of protein mixtures are greatly needed. Besides, unlike chromatographic methods where motion of the proteins thorough a stationary phase packed in a column is given by pumping a mobile phase through it, microfluidic devices based on electrokinetic forces are able to move the sample along with the fluid thorough the channel without other external forces. Thus, the physics governing the movement of proteins inside a microfluidic system are more complex and poorly understood. Therefore, the development of computational models to simulate microfluidic systems is of utmost importance to improve the design of such devices in the route of establishing micro-bioseparation strategies.

Electrophoresis (EP) and electroosmosis (EO) are two phenomena that take place in an electrokinetically driven microfluidic device. EP acts upon charged particles, while EO acts on a fluid that is in contact with an electrically charged surface (e.g., the walls of a microfluidic channel). The EP and EO forces are generally grouped into a single EK force ($\vec{F}_{EK}$) acting on the particles. The magnitude of this force greatly depends on the electric properties of the device and particles as well as on the electric and mechanical properties of the suspending fluid. Besides the $\vec{F}_{EK}$, the motion of the proteins inside the channel is also influenced by the dielectrophoretic force ($\vec{F}_{DEP}$) that occurs when particles suspended in a fluid polarize under inhomogeneous electric fields.[14] Thus, the net motion of the protein particles is given by a balance between these two forces. In fact, the magnitude of these forces is mainly determined by the electric properties of the fluid and the particles such as conductivity and permittivity. Additionally, the size of the particles and the distribution of the electric field throughout the microfluidic channel have great impact on the magnitude of $\vec{F}_{DEP}$.

Recently, we have proposed a Direct Current (DC) insulator-based dielectrophoresis (iDEP) microfluidic system as an alternative to manipulate PEGylated proteins.[15] In iDEP systems, arrays of insulating structures are embedded within the microfluidic channel and an electric field is generated through the application of a voltage between two distant electrodes inserted in the inlet and outlet of the device. The insulating structures deform the electric field creating non-uniform DC fields that polarize particles.[9] So far, we have demonstrated that mono-PEG and di-PEG RNase A conjugates can be captured and concentrated in one single step at different voltages using iDEP microchannels, while the native protein is not captured at any of the conditions tested.[15] Nonetheless, in our previous work, we did not describe the electrokinetic phenomena involved in this system.

Modelling is an important step in the design of devices as it provides valuable information that allows the prediction of the behavior of particles in a determined system under specific conditions. In addition, this information allows the design of specific experiments, not requiring the exploration of every experimental condition, thus saving time and resources. Furthermore, the study of heat transfer inside microfluidic channels is of primary importance when biological molecules are attempted to be manipulated via iDEP. This is because the high voltages applied

to the microfluidic system rise the fluid temperature considerably, which may have an irreversible effect on the protein, resulting in a lack of biological activity.

Considering the importance of mono-PEG RNase A, we now present a detailed description of the main forces acting on this PEG-protein conjugate under DC-voltages inside iDEP microdevices. In doing so, we developed a 3D-model of the electrokinetic phenomena for mono-PEG RNase A in order to understand the physics that govern the system presented here. Additionally, we also present a model that simulates the behavior of the native protein. Moreover, we have also modeled the temperature rise within the iDEP device and studied the effect it has on important electric and mechanic properties of the fluid (dynamic viscosity, electrical conductivity, and thermal conductivity). We consider that this work will allow the design of devices with a major efficiency towards the isolation and recovery of this and other proteins.

II. MATERIALS AND METHODS

A. EK models

To study the dielectrophoretic response of native RNase A to a DC electric field, we modelled this protein as an sphere.[16] The dielectrophoretic force, $\vec{F}_{DEP}$, exerted on a spherical particle is given by[14]

$$\vec{F}_{DEP} = 2\pi\varepsilon_m r_p^3 Re(f_{CM})\nabla E^2. \tag{1}$$

In the above equation, ε_m is the permittivity of the fluid, r_p is the radius of the particle, ∇E^2 is the gradient of the electric field squared, and $Re(f_{CM})$ is the real part of the Clausius-Mossotti factor. Under DC electric fields, the latter can be expressed in terms of the electric conductivities of the particle (σ_p) and suspending medium (σ_m)[17]

$$Re(f_{CM}) = \frac{\sigma_{p-}\sigma_m}{\sigma_p + 2\sigma_m}. \tag{2}$$

From the above equation, it is clear that the Clausius-Mossotti factor can take on positive or negative values as a function of the conductivities of the particle and medium. This gives rise to two different dielectrophoresis (DEP) modes, positive or negative DEP. The former occurs when particles are driven to regions of high electric fields, while the latter happens when particles are repelled from the same zones. In response to $\vec{F}_{DEP}$ exerted on the particles, these will move with a velocity $\vec{v}_{DEP}$ given by[18]

$$\vec{v}_{DEP} = \mu_{DEP}\nabla E^2\,, \tag{3}$$

where μ_{DEP} describes the dielectrophoretic mobility, which can be expressed as

$$\mu_{DEP} = \frac{r_p^2\varepsilon_m f_{cm}}{3\eta}, \tag{4}$$

with η representing the dynamic viscosity of the medium.

To model the mono-PEG RNase A electrokinetic phenomena, the conformation of the PEG chain should be taken into consideration under two possible scenarios. It may be assumed that the PEG chain wraps the protein molecule as a shroud (assuming a spherical model) or that it remains as an extended random coil (assuming a dumbbell model). In this context, there are some reports supporting the dumbbell conformation for mono-PEG RNase.[19] Besides, studies of PEG conformation in lysozyme, which is similar to RNase A in size and form, have also supported a dumbbell conformation.[20] Since there is no mathematical description for a dumbbell geometry, we approximated it through an elliptical geometry that has been previously adapted for IgG and yellow fluorescent proteins.[21,22] The equation that describes the dielectrophoretic force, $\vec{F}_{DEP}$, acting on an ellipse-shaped particle can be written as follows:

$$\vec{F}_{DEP} = \frac{4}{3}\pi abc\varepsilon_m f_{mCM}\nabla E^2. \tag{5}$$

In the above equation, a, b, and c represent the radius of the particle (being $b = c$ and $a > b$) for the x, y, and z axes, respectively, and are used to calculate the volume of the particle. The term f_{mCM} corresponds to the modified Clausius-Mossotti factor, which can be calculated using the following equation:

$$f_{mCM} = \frac{\sigma_{p-}\sigma_m}{Z\sigma_p + (1-Z)\sigma_m}, \tag{6}$$

where Z stands for the geometrical polarization relaxation factor, defined as

$$Z = \frac{bc}{2a^2e^3}\left[ln\left(\frac{1+e}{1-e}\right) - 2e\right], \tag{7}$$

with $e = \sqrt{1-(bc/a^2)}$ and represents the eccentricity.

The dielectrophoretic force also induces particle motion for ellipse-shaped particles, and these move with a dielectrophoretic velocity given in Equation (3). Nonetheless, the μ_{DEP} term has a different form than that of Equation (4). For ellipse-shaped particles

$$\mu_{DEP} = \frac{2abc\varepsilon_m f_{mCM}}{9\eta\bar{R}}. \tag{8}$$

The mean translational coefficient, $\bar{R}$, in Equation (8) is calculated from $\bar{R} = 2/S$, where S is described as

$$S = \frac{2}{\sqrt{a^2-b^2}}ln\left[\frac{a+\sqrt{a^2-b^2}}{b}\right]. \tag{9}$$

In addition to DEP, electroosmosis and electrophoresis are other transport mechanisms that contribute to particle motion with velocities $\vec{v}_{EO}$ and $\vec{v}_{EP}$, respectively. In this work, microchannels were made of polydimethylsiloxane (PDMS), a material with a predominating negatively charged surface. Thereby, the EK velocity ($\vec{v}_{EK}$) can be described as follows, in terms of the EO and EP velocities[23]

$$\vec{v}_{EK} = \mu_{EK}\vec{E} = (\mu_{EO} + \mu_{EP})\vec{E}, \tag{10}$$

$$\vec{v}_{EO} = \mu_{EO}\vec{E}, \tag{11}$$

$$\vec{v}_{EP} = \mu_{EP}\vec{E}, \tag{12}$$

where μ_{EO} and μ_{EP} represent the electroosmotic and electrophoretic mobilities, respectively. Both mobilities can be estimated from the Helmholtz-Smoluchowski equation[24]

$$\mu_{EP} = \frac{\varepsilon_m\zeta_p}{\eta}, \tag{13}$$

$$\mu_{EO} = -\frac{\varepsilon_m\zeta_s}{\eta}, \tag{14}$$

where ζ represents the zeta potential for the particle (p) and the microfluidic channel walls (s), respectively.

To reach protein particle capture, the magnitude of the dielectrophoretic velocity must be superior to that of the electrokinetic velocity, including motion by diffusion. By assuming that DEP and EK are the dominant transport mechanisms contributing to particle motion, neglecting

the effect of diffusion, and with C, a correction factor that accounts for unconsidered phenomena and experimental errors, particle trapping zones within the microfluidic channel are defined as

$$\frac{C|\vec{v}_{DEP}|}{|\vec{v}_{EK}|} > 1. \tag{15}$$

In addition, we have considered Joule heating phenomenon in our model in order to study the temperature distribution within our microfluidic channels and avoid damaging the sample during the experiments. The effect of temperature increments in the electrical, thermal, and mechanical properties of the fluid (which affect particle velocity) was studied. A detailed description of the Joule heating model is presented in Sec. II B.

B. Solving the models

All the equations describing the various electrokinetic phenomena considered here were computed in COMSOL Multiphysics v5.1 (COMSOL, Inc., Burlington, MA, USA). The distributions of $\vec{E}$ and ∇E^2 along the microchannel were simulated by solving the Laplace equation using the Electric Currents module. The temperature across the channel was calculated considering heat transfer in the fluid (solution) and in the solid (PDMS) phase. This was performed using the Multiphysics and Heat Transfer modules. The definitions of the domains and boundary conditions employed in our model are presented in Figure 1 and Table I, respectively.

To solve the model, a custom free tetrahedral mesh calibrated for general physics was created in our 3D geometry. The maximum and minimum mesh element sizes were set to 5000 μm and 40 μm, respectively, with a maximum element growth factor of 1.4 and curvature factor of 0.4. The resolution of narrow regions was set to a value of 0.65. A time dependent study was performed in our model. For the properties of the PDMS and suspending solution (water), the COMSOL Material Library was used. The input data used in each COMSOL module are listed in Table II. The radius of the native RNase A was obtained from literature, while the data

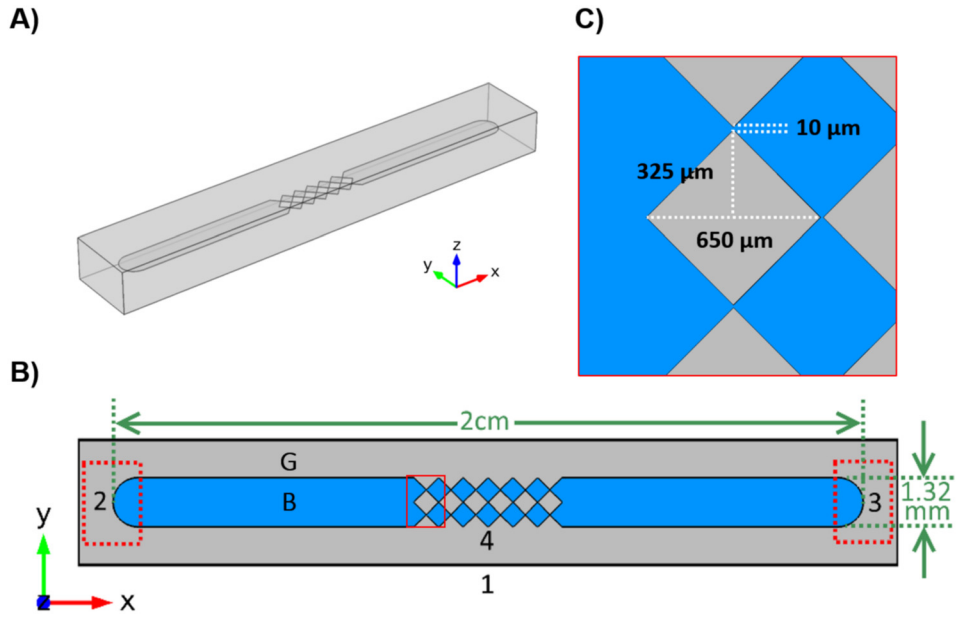

FIG. 1. Schematic diagram of the microfluidic device in (a) 3D and (b) 2D perspective. Numbers in (b) indicate the boundary conditions employed in our model. (c) Zoomed-image of a region of the microfluidic channel showing the dimensions of the diamond-shape insulating structures and the gap. The gray region (G) represents the PDMS domain, and the blue region (B) represents the fluid domain. Boundary 1 represents the outer PDMS surface (including the external top and bottom faces of the PDMS). Boundaries 2 and 3 represent the PDMS/fluid interface where the electric stimulus is applied (restricted to the zones within dotted boxes in the figure). Boundary 4 represents the remaining PDMS/fluid interface (including top and bottom faces of the channel).

TABLE I. Conditions, definitions, and input data used in COMSOL models. $\vec{J}$ is the electric current, $Q_j = -\frac{d\rho_v}{dt}$ (where ρ_v represents the volume charge density), $\vec{J}_e$ is an external electric current density, $Q = Q_b$, $Q_b = \vec{J} \cdot \vec{E}$, $Q_{vd} = \tau : \nabla\vec{v}$ accounts for viscous dissipation, $Q_p = \alpha_p T\left(\frac{\partial p}{\partial t} + \vec{v} \cdot \nabla p\right)$, α_p is the coefficient of thermal expansion, and $Q_e = \frac{1}{2}\left[\mathrm{Re}(\vec{J} \cdot \vec{E}) + Re\left(j\omega\vec{B} \cdot \vec{H}\right)\right]$.

Module	Element	Definition
Electric currents		
Current conservation	B and G	$\nabla \cdot \vec{J} = \mathrm{Q}_j; \vec{J} = \left(\sigma + \varepsilon_0\varepsilon_r\frac{\partial}{\partial t}\right)\vec{E} + \vec{J}_e; \vec{E} = -\nabla \mathrm{V}$
Electric insulation	1	$\vec{n} \cdot \vec{J} = 0$
Initial values	B and G	$V_0 = 0$
Electric potential	2	$\phi = \phi_{inlet}$
Ground	3	$\phi = 0$
Heat transfer		
Heat transfer in fluids	B	$\rho C_p\left(\frac{\partial T}{\partial t} + (\vec{v} \cdot \nabla T)\right) = \nabla \cdot (k\nabla T) + Q$
Heat transfer in solids	G	$\rho C_p\left(\frac{\partial T}{\partial t} + (\vec{v} \cdot \nabla T)\right) = \nabla \cdot (k\nabla T) + Q + Q_{vd} + Q_p$
Initial values	B and G	$T_0 = 20\,^\circ\mathrm{C}$
Temperature 1	2	$T = T_0$
Diffuse surface	1	$-\vec{n} \cdot (-k\nabla T) = 0.9\sigma(T_0^4 - T^4)$
Multiphysics		
Electromagnetic heat source	B and G	$\rho C_p\left(\frac{\partial T}{\partial t} + (\vec{v} \cdot \nabla T)\right) = \nabla \cdot (k\nabla T) + Q_e$
Boundary electromagnetic heat source	1–4	$-\vec{n} \cdot (-k\nabla T) = Q_b$

related to the sizes of the semi-axes (a, b, and c) for the mono-PEGylated RNase A were approached from values reported for mono-PEG lysozyme, being the native lysozyme similar in size to native RNase A. Note that the PEG chemistry used to PEGylate the lysozyme is the same we used in this work to modify RNase A. Also, since the electric properties of the RNase A have not been reported in the literature, in the present study, we assumed the electric conductivity of the protein to be similar to that of lysozyme. Both native and mono-PEGylated RNase A showed no differences in the pI value (data not shown). Because of this, the electric conductivity

TABLE II. Input parameters used for COMSOL simulations.

Parameter	Value	Units
Radius of the native RNase, r[a]	1.5×10^{-9}	m
a-semiaxis of mono-PEG, a[b]	21.4×10^{-9}	m
b-semiaxis of mono-PEG, b[b]	3.5×10^{-9}	m
c-semiaxis of mono-PEG, c[b]	3.5×10^{-9}	m
Electric conductivity of RNase A, σ_p[c]	0.10	S/m
Initial electric conductivity of the medium, σ_{m0}	0.01	S/m
Conductivity density incremental factor, α	0.02	1/°C
Permittivity of medium, ε_m	80	1
Zeta potential of RNase A, ζ_p[d]	−0.01, 0, +0.01	V
Zeta potential of PDMS, ζ_{PDMS}[e]	−0.013	V

[a]Value was obtained from Ref. 16.
[b]Values were taken from Ref. 20.
[c]Value was calculated from Ref. 25.
[d]Values were set according to Ref. 26.
[e]Value taken from Ref. 27.

of the native and mono-PEGylated RNase A was assumed to be the same. Zeta potential values for PDMS and proteins were set according to experimental data obtained from literature.

It must be noted that the electric conductivity of the medium, σ_m, is a function of the initial electric conductivity of the medium, σ_{m0}; the initial temperature, T_0; the temperature, T; and the conductivity density incremental factor, α; and it is defined as: $\sigma_m = \sigma_{m0}(1 + \alpha(T - T_0))$.

C. Parametric study

As the electric properties of the proteins, such as the ζ_p and conductivity σ_p, depend to a great extent on the ionic strength and pH of the surrounding medium, it is important to study how the combination of these properties impacts the dielectrophoretic behavior of the proteins inside a microfluidic channel. It has been reported that RNase A ζ_p can vary from −0.010 to 0.010 V approximately under different conditions of ionic strength and pH.[26] So far, there is lack of literature reporting conductivity of proteins, especially for RNase A, although there are some reported values available for other proteins that vary in a very wide range.[22,28–30] As we experimentally observed streaming or trapping DEP for both proteins (native and PEGylated) in positive mode, we set $\sigma_p = 1000\,\mu$S/cm, one order of magnitude higher than σ_m, to guarantee positive DEP theoretical predictions. Besides, we varied σ_p up to 10 000 μS/cm with no significant changes in the EK velocity response (data not shown). To explore the effect of the protein electric properties on their electrokinetic velocity responses, we ran a parametric study in COMSOL by varying ζ_p from −0.01 to 0.01 V. The parameters σ_p, σ_m, ζ_{PDMS}, and ε_m were set to the values indicated in Table II. The outcome of this study will be presented and discussed in Section III D.

D. The device

The microchannel was designed with Autodesk AutoCAD® 2014 student version (©2013 Autodesk, Inc., USA) and patterned on PDMS using soft photolithography. The details of design are shown in Figure 1, and the details of the microfluidic channel fabrication are described in Mata-Gómez *et al.*[15]

E. Sample preparation

The mono-PEG RNase A conjugate was synthesized by modifying the native RNase A (Cat. No. R500) with methoxy-PEG-propionaldehyde of 20 kDa (Cat. No. M-ALD-20 K, Jenkem Technology).[31] The mono-PEG RNase A conjugate was isolated from the PEGylation reaction by SEC.[31] The native and the pure conjugate proteins were stained separately with fluorescein isothiocyanate (FITC, Cat. No. 46950, Sigma) as described before.[15] Reaction mixtures were adjusted to 2.5 ml and loaded onto a PD10 desalting column to remove FITC excess and eluted using K_2HPO_4 buffer at a conductance of 100 μS/cm and pH 8. Samples were stored at −20 °C until used.

F. Experimental set-up

Prior to performing the experiments, the surface of the microfluidic channel was treated with 100 mM NaOH, rinsed and conditioned with K_2HPO_4 buffer at a conductance of 100 μS/cm and pH 8. Micro-filtered samples were introduced into the channel. Electrodes of platinum wire, 0.584 mm diameter, were placed into the reservoirs. A DC electric potential was applied using a high-voltage sequencer (LabSmith, Livermore, CA, USA). All iDEP experiments were recorded in video format with an AxioCam MR video camera connected to a fluorescence Axio Vert 1 microscope (Carl Zeiss, Germany) equipped with a filter set No. 49 (445/50 nm) and the AxioVision software (Carl Zeiss, Germany). Both, the microscope and the voltage sequencer required the use of a personal computer.

III. RESULTS AND DISCUSSION

A. Simulation and experimental dielectrophoresis of the proteins

During experimental runs, native protein was not trapped at any of the voltages tested (2500, 3000, 3500, and 4000 V). Instead, RNase A was observed to move freely from anode to cathode as a consequence of the electroosmotic flow present in the microfluidic channel. Figure 2 presents the experimental and simulated results of the electrokinetic behavior of native RNase A. Although dielectrophoretic trapping was not attained at any applied voltage, weak streaming behavior was observed, since $\vec{F}_{DEP}$ is strong enough to overcome diffusion forces but $\vec{F}_{EK}$ continues to dominate the system, and particles are focused along different regions.

Figures 2(b)–2(d) depict a slight trace of protein molecules concentrated along the array of posts when the device was stimulated with DC voltages of 3000, 3500, and 4000 V, right at the fluid side of the PDMS/fluid interface, as evidenced by the increase in fluorescence intensity (greener areas) at the mentioned regions. Similar observations were obtained by a different research team, which reported that IgG protein particles were focused alongside the posts inside an iDEP microfluidic device, cataloguing the behavior as streaming DEP.[32] Simulations of the electrokinetic phenomena for the native protein, which considered a correction factor, C, ranging from 200 to 270, are also presented in Figure 2. Surface plots shown in Figures 2(e)–2(h) describe the resultant velocity magnitude (in a logarithmic scale) of the various electrokinetic phenomena occurring in the channel when the protein is subjected to a DC electric field.

The zoomed images in Figures 2(i)–2(l) show the magnitude (surface plot) of the total velocity and its direction (arrows). It is important to mention that arrows in the plots only indicate the direction of the resultant particle velocity but do not indicate protein particle distribution. Note that in these figures all the arrows point towards one direction, the cathode, and there are no arrows pointing in the opposite direction. This suggests a dominance of the electroosmotic flow in the system. In other words, the magnitude of the dielectrophoretic force is not strong enough to counteract the action of the electroosmotic force under the conditions tested. Thus,

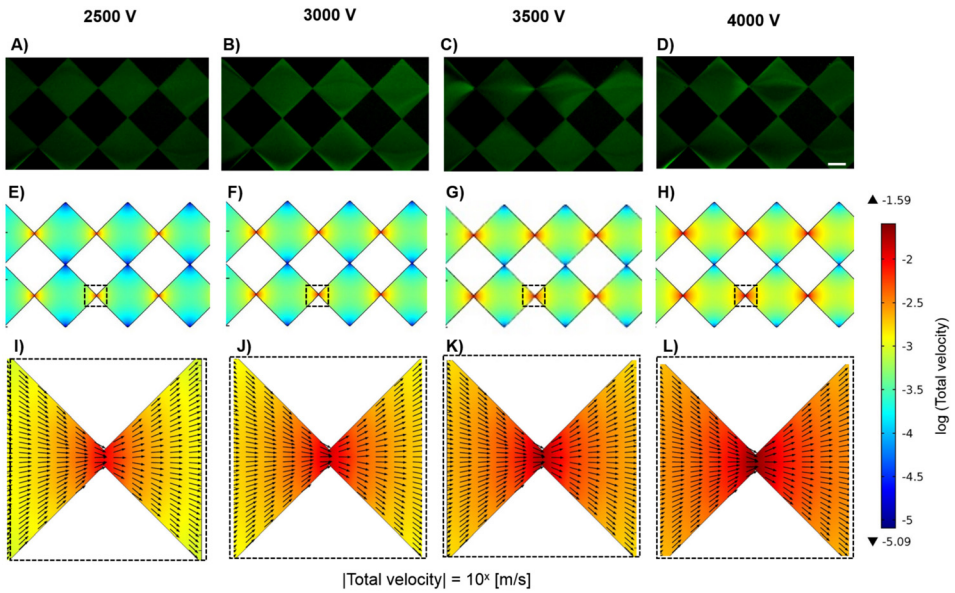

FIG. 2. (a)–(d) Experimental results showing FITC-stained native RNase A protein experiencing particle streaming at 2500, 3000, 3500, and 4000 V. The microchannel was filled with a phosphate buffer with pH 8 and at a conductivity of 100 μS/cm. Flow is from left to right. Scale bar is 200 μm. (e)–(h) Surface plots showing the magnitude of the theoretical total particle velocity. Total velocity was calculated as the sum of the electrophoretic, electroosmotic, and dielectrophoretic velocities contributing to protein transport in the microfluidic system. (i)–(l) Arrow plots of the total velocity from the zoomed-in images of the gap zone between the insulator tips delimited by the dashed squares. Both images experimental and simulated were obtained after 30 s of electric stimulation.

the trapping condition described in Equation (15) is not fulfilled and thereby trapping is not achieved.

The weak streaming behavior observed at the fluid side of the PDMS/fluid interface must therefore be a result of particle focusing from positive DEP and the no-slip boundary condition that governs the behavior of fluids in contact with a surface, which creates low-velocity regions close to it. These regions can be observed in Figures 2(e)–2(h) as depicted by the blue regions at the channel walls. Simulation predictions presented here are in good agreement with the experimental evidence and provide an explanation for the lack of native RNase A trapping. To achieve trapping, the magnitude of the dielectrophoretic velocity must overcome the magnitude of the combined velocity due to electroosmosis and electrophoresis, but, at the conditions tested for the native RNase protein, the dielectrophoretic force is only stronger than the diffusion forces.

Mono-PEG RNase A also experienced streaming-like dielectrophoresis at 2500, 3000, and 3500 V (Figures 3(a)–3(c)), although stronger than that experienced by the native protein (see Figure 2). The streaming pattern is more evident in Figure 3(c) where protein particles focused alongside of the insulators as well as on the walls of the channel as evidenced by the more intense fluorescence in these regions. In contrast to the results obtained with the native protein, mono-PEG RNase A was experimentally captured at 4000 V as illustrated in Figure 3(d). In this micrograph, it is observed that protein particles were concentrated at the small gaps within the channel after applying the electric stimulus for 30 s.

The ellipse model used to study the electrokinetic response of the PEGylated protein allowed the theoretical prediction of the magnitude (Figures 3(e)–3(h)) and direction (Figures 3(i)–3(l)) of the protein velocity within the microfluidic channel. As shown in Figure 2, this velocity plot has a logarithmic scale and takes into account the contributions of electrophoresis, electroosmosis, and dielectrophoresis to particle motion as well as a correction factor ranging from 200 to 270. In Figures 3(i)–3(k), we show that at the narrowest regions of the microfluidic channel, the trapping condition described in Equation (15) is still not satisfied up to an applied voltage of 3500 V. This is evidenced by the presence of velocity vectors pointing toward the PDMS surface but with none of them pointing in the opposite direction to the EK velocity. This is in agreement with the

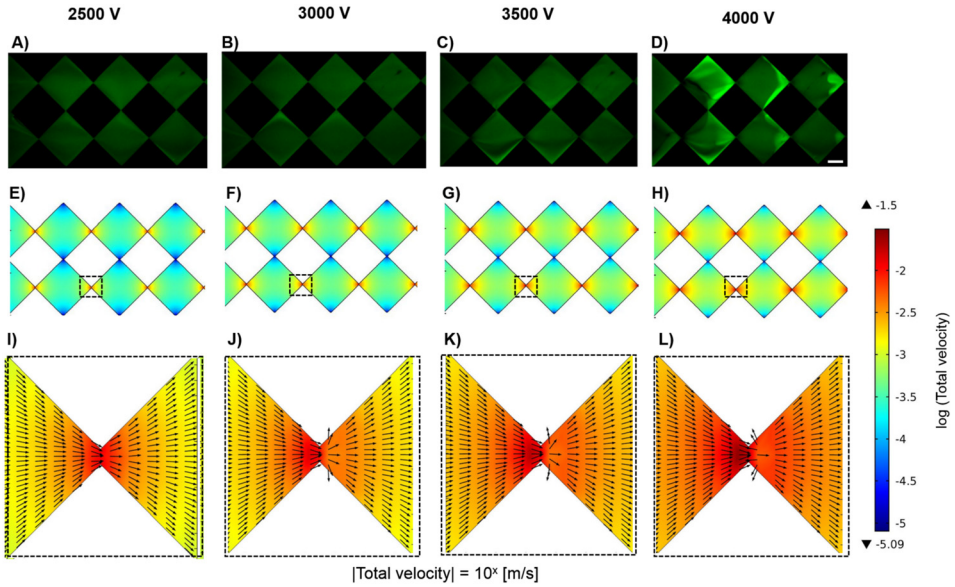

FIG. 3. (a)–(d) Experimental results showing FITC-stained mono-PEGylated RNase A experiencing streaming or trapping due to positive dielectrophoresis at 2500, 3000, 3500, and 4000 V. The microchannel was filled with a phosphate buffer with pH 8 and at a conductivity of 100 μS/cm. Flow is from left to right. Scale bar is 200 μm. (e)–(h) Surface plots showing the total theoretical velocity and its magnitude. Total velocity was calculated as the sum of the electrophoretic, electroosmotic, and dielectrophoretic velocities contributing to protein transport in the microfluidic system. (i)–(l) Arrow plots of the total velocity from the zoomed-in images of the gap zone between the tips of the insulators delimited by the dashed squares. Both images experimental and simulated were obtained after 30 s of electric stimulation.

experimental observation of the dielectrophoretic streaming with a higher intensity than that observed for the native protein (refer to Figures 2(a)–2(d) and 3(a)–3(c)).

In contrast, when a DC voltage of 4000 V is considered in our computational model, velocity vectors right after the channel constrictions point towards the constrictions (in the opposite direction to the EK velocity) as shown in Figure 3(l), indicating particle trapping. As shown in Figure 2, note that arrows only indicate the direction of the resultant particle velocity magnitude and not the distribution of protein particles. For this reason, the experimental results do not entirely match the simulated results, at least visually. However, the fact that arrows point to the gap at both sides of the gap does suggest that the DEP velocity is greater than the EK velocity at that region, favoring protein capture. Therefore, simulated results are in good agreement with the experimental observations.

It is worth mentioning that values for the correction factor, C, in Equation (15) as high as 600 have been considered in the past while studying the electrokinetic response of much larger particles. Moreover, previous works exhibit a trend in the values assigned to the correction factor, i.e., the smaller the particle, the higher the correction factor.[33–35] For example, for polystyrene beads with diameters of 1 and 4 μm, correction factors of 600 and 100 were required, respectively, to predict DEP trapping.[33] The slope of a correction factor versus particle diameter plot for that work would have a value of -166.667×10^6 (1/m). Assuming the ideal case in which the correction factor is a linear function of particle diameter, the correction factor required to predict protein particle trapping would have a value in the 750–800 range. Therefore, the use of correction factors ranging from 200 to 270 to predict nanometer-sized protein particles trapping in iDEP-based devices, as in our case, represents an improvement in the model prediction accuracy. We argue that this improvement is due to the consideration of a 3D geometry instead of a much simplified 2D geometry as well as to the consideration of heat transfer phenomena (Joule heating). A similar approach has been employed by Nakano *et al.*, where the authors estimated the dielectrophoretic mobilities for β-galactosidase that led to a good agreement between experimental observations and computational predictions.[36] They reported dielectrophoretic mobilities in the range of $10^{-21}\,m^4/V^2\,s$. The product of our calculated dielectrophoretic mobilities and proposed correction factor, C, lies in the range of $10^{-21}\,m^4/V^2\,s$ and is therefore in good agreement with such approach.

According to our model, mono-PEG RNase A exhibited DEP in positive mode since velocity vectors pointed in the direction of high electric field regions. This observation is in agreement with the experimental observations since captured protein was accumulated at the zones of highest electric field gradients, i.e., near the tips of the diamond-shaped insulators as depicted in Figure 3(a).

To further reduce the correction factor used in our model, other important aspects should be considered, for example, pH. It is known that pH gradients form under high external electric stimulis.[37] The pH affects EK phenomena,[23] which in turn impacts the total particle velocity. Moreover, Brownian motion has been shown to play a significant role in particle manipulation dynamics for sub-micrometer particles and therefore should also be considered in a model.[38]

B. Heat transfer distribution inside the microchannel

Temperature is a parameter greatly related to the activity of biological molecules. In our experiments, we have applied high voltages to achieve dielectrophoretic capture of the PEGylated species. A consequence of the application of high voltages in microfluidic devices is temperature rise due to Joule heating. Therefore, it is of vital importance to study heat transfer phenomena inside microfluidic channels to guarantee the permanence of protein biological activity after being subjected to dielectrophoretic manipulation. Predictions of the temperature distribution inside the microchannel, obtained via computational modelling, at four different electric potentials (2500, 3000, 3500, and 4000 V) are presented in Figure 4.

Since the power dissipated by Joule heating in any point within the microfluidic channel is proportional to the square of the electric field at that point, the temperature rises in the regions located between the tips of the insulators (hot-spots) was steeper than in any other regions of the device (Figures 4(a)–4(d)). See zoomed-in images in Figures 4(e)–4(h) for a detailed view of the temperature distribution at a hot-spot. Moreover, it is important to note that the temperature in the

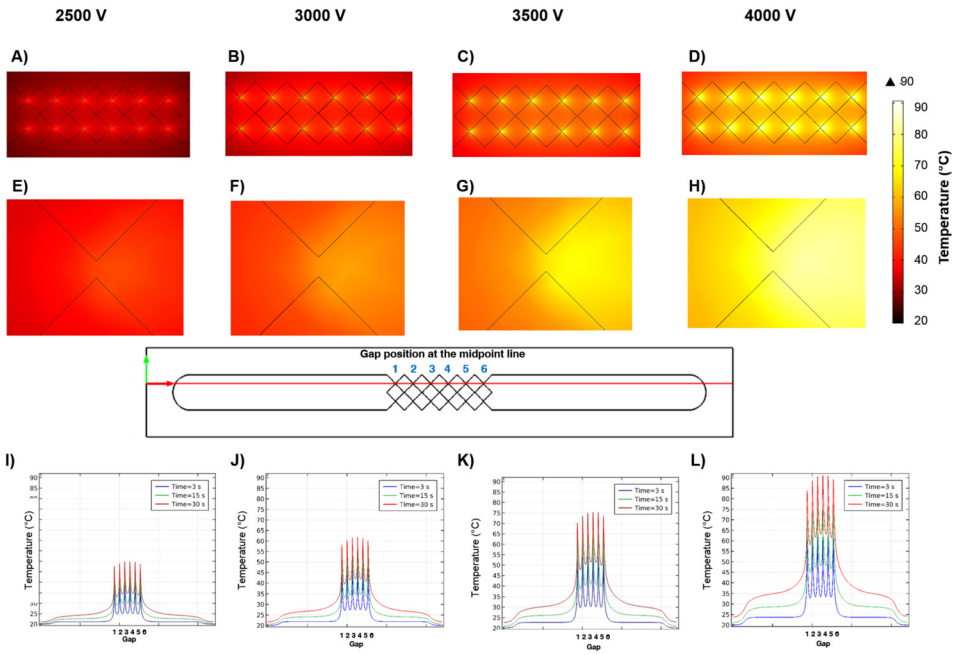

FIG. 4. Distribution of the temperature inside the microchannel. (a)–(d) 2D surface plot showing the hot-spots at the gap zones after applying 2500, 3000, 3500, and 4000 V for 30 s. (e)–(h) Zoomed-images of a microchannel gap showing the distribution of the temperature at the hot-spot. (i)–(l) Temperature distribution along the cut-line depicted in the schematic drawing as a function of time.

hot-spots at the gaps depicted in the schematic drawing in Figure 4 increased considerably as a function of time when the applied voltage was changed from 2500 to 4000 V (Figures 4(i)–4(l)). Maximum temperature (∼90 °C) was achieved at the third and fourth hot-spots after the solution was exposed to an electric field generated through an electric potential of 4000 V for 30 s (Figure 4(l)).

Recently, Nakano *et al.* published experimental measurements of temperature in a device with insulating posts (although the shape and dimensions are different from those of our design) that show a similar trend than our predictions.[39] According to the information provided by the supplier, RNase A can be stable up to 100 °C in its native form. Besides, it has been demonstrated that grafting of PEG molecules onto lysozymes increased their thermal stability retaining their activity up to 90%.[40] PEG chains grafted to the protein, therefore, protect it from being denatured by heat, keeping its chemical structure intact, and preserving its biological activity. Lysozyme has similar size and structure to RNase A. Thus, owing to the PEG chains grafted to it, PEGylated RNase A may exhibit a similar increase in thermal stability as compared to PEGylated lysozyme, but better than native RNase A.

It is noteworthy that, although trapping of PEGylated RNase A starts right after the application of a 4000 V electric potential to the microfluidic device, a significant enrichment of the protein was only achieved after ∼15 s of sustained electric stimulus (refer to Figure 3). Hence, at that moment the temperature of the solution is expected to be ∼80 °C. Therefore, along with the evidence of the thermal stability of some other PEGylated proteins reported in the literature, our computational predictions indicate that the temperature of the solution during our dielectrophoretic manipulation experiments will not have an impact on the biological activity of the PEGylated RNase A. Note that even though temperature continued to increase after 30 s of electric stimulus, the trapping occurred in a shorter time, thus we can still use this device without affecting the biological activity of the protein.

C. Temperature impact onto trapping related parameters

Dielectrophoretic manipulation (in this work: streaming or trapping) of particles strongly depends on several material parameters whose values are a function of temperature. One of

those parameters is the electric conductivity of the suspending solution. Figure 5(a) illustrates the change in electric conductivity, $\Delta\sigma_m$, after 30 s of electric stimulation with a DC voltage of 4000 V ($\sigma_m = 100\,\mu$S/cm at t = 0). It can be seen that $\Delta\sigma_m$ increases at the temperature hot-spots (refer to Figure 4) and reaches a maximum value of 140 μS/cm at t = 30 s. This means that in those spots, $\sigma_m = 240\,\mu$S/cm after 30 s of the electric stimulation. Equations (1) and (5) show that the DEP force is a function of the suspending solution electric conductivity through the Clausius-Mossotti factor, whose value decreases (and may even become negative) with higher values of σ_m. Therefore, it is expected that as a trapping experiment is carried out, the intensity of streaming or trapping will decrease with time. Thus, the effect of sample temperature rise *via* Joule Heating has a negative impact in the dielectrophoretic response of the proteins in our microfluidic device.[35]

The dynamic viscosity of the suspending solution, η, is another parameter with a significant role in the dielectrophoretic streaming or trapping of particles (refer to Equations (4) and (8), where μ_{DEP} is defined). Because μ_{DEP} is inversely proportional to the suspending solution dynamic viscosity, the dielectrophoretic velocity of the particles decreases with larger values of η and increases with smaller values of η. Figure 5(b) illustrates the change in dynamic viscosity experienced by the suspending solution as a function of temperature ($\eta = 1.01\,\text{mN/m}^2\,\text{s}$ at t = 0). In contrast to the change in electric conductivity shown in Figure 5(a), which is positive, the change in dynamic viscosity is negative. After 30 s of electric stimulus with a DC voltage of 4000 V, $\Delta\eta = -6.96 \times 10^{-4}\,\text{mN/m}^2\,\text{s}$, meaning that $\eta = 0.314\,\text{mN/m}^2\,\text{s}$ at t = 30 s (only 31% of its value at t = 0). Owing to this decreased dynamic viscosity, the dielectrophoretic response of the proteins is expected to improve with time through a reduction of the drag coefficient acting upon the particles. The fact of having inverse responses in the change of electric conductivity and in the change of dynamic viscosity definitely reduces the impact of these combined phenomena on the dielectrophoretic force. However, as reported by Gallo-Villanueva *et al.*, the effective intensity of the DEP trapping slightly reduces with time.[35]

Finally, the thermal conductivity, k, of the suspending solution is also a function of temperature. This property is of interest particularly as it controls the rate at which the fluid heats due to an external heat source (electricity in the present scenario). Moreover, for our present application, an increment in the thermal conductivity of the solution will be beneficial, as it will be more difficult to heat the solution (producing a smaller ΔT) and the proteins will remain active. In Figure 5(c), we show the change in thermal conductivity, Δk, experienced by the suspending solution in our microfluidic channel after 30 s of exposure to an electric field generated by an applied DC voltage of 4000 V ($k = 0.49\,\text{W/m K}$ at t = 0). Δk takes on a maximum value of $0.08\,\text{W/m K}$ at the temperature hot-spots, representing an increment of 16.3% in comparison with the value of k at t = 0. It must be noted that the change in these three material parameters as a function of temperature has been taken into account while calculating the temperature distribution and total velocity of the proteins in our microfluidic channel.

D. Parametric sweep study

The magnitude of the electric potential in the electrical double layer, formed atop a charged surface, at the location of the slipping plane, ζ, is a relevant parameter that influences the balance

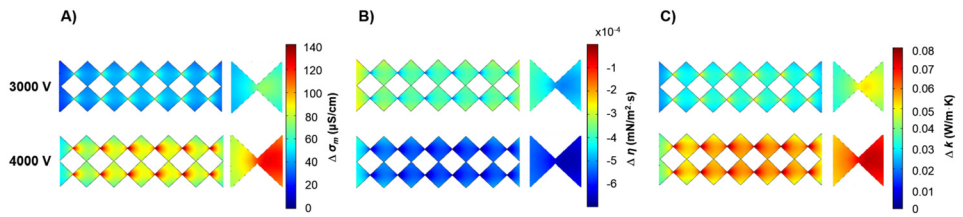

FIG. 5. Impact of temperature on the electric and mechanic properties of the suspending solution that are related to particle trapping (an enlarged view of a single constriction appears to the right of each surface plot). (a) Electric conductivity, σ_m; (b) dynamic viscosity, η; and (c) thermal conductivity, k. Images were obtained considering 30 s of electric stimulation.

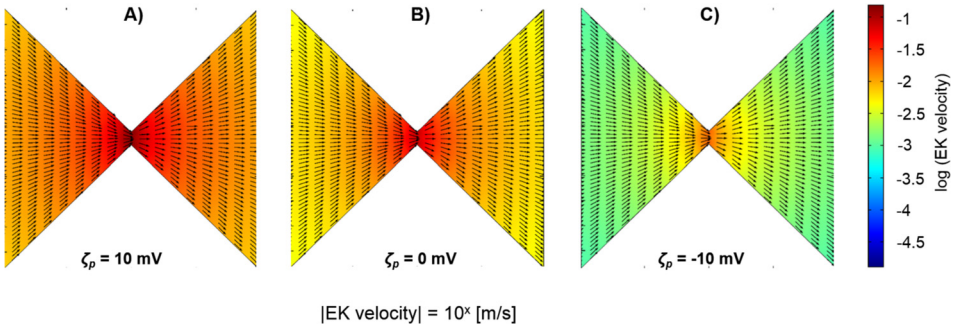

FIG. 6. Enlarged views of a single constriction (the narrowest region) inside the channel showing electrokinetic velocity as a function of protein zeta potential (ζ_p). A ζ_{PDMS} value of -13 mV was considered for the simulations. (a) $\zeta_p = 10$ mV, (b) $\zeta_p = 0$ mV, (c) $\zeta_p = -10$ mV. Images were obtained considering 5 s of electric stimulation at 4000 V.

between the EP and EO mobilities (refer to Equations (13) and (14)). The zeta-potential of a particle, ζ_p, is related to the particle net-charge. A change in ζ_p affects the overall EK velocity, which in turn affects the dielectrophoretic trapping condition defined in Equation (15). Because of this, it is important to know what values ζ_p may take under certain experimental conditions.

For a protein, the value of ζ_p varies as a function of the pH of the suspending solution, as it influences protein net charge.[26,41] To the best of our knowledge, to the time of writing of this paper, no mathematical model that calculates ζ_p as a function of pH is available in the literature. Therefore, we performed a parametric sweep study to find out what values of ζ_p favored our model by reducing the resultant EK velocity. The range of values for ζ_p (between -10 and 10 mV) fed to the model was selected according to a previous investigation where it was demonstrated that the zeta-potential of native RNase A takes on positive values in acidic buffers or negative values in neutral or basic buffers.[26]

Computational predictions of the impact of ζ_p on the EK velocity are shown in Figure 6. The highest EK velocity, with a magnitude of 0.1 m/s, was obtained for a $\zeta_p = 10$ mV at the narrowest regions of the microfluidic channel (at the tips of the diamond-shape posts). In this case, both EO and EP point in the same direction as the electric field, thus the sum of their contribution to protein transport results in a higher EK velocity and therefore the ratio in Equation (15) takes on lower values (see Figure 6(a)). In contrast, when $\zeta_p = -10$ mV, EK velocity was considerably reduced up to 10 times, compared to the EK velocity obtained with $\zeta_p = 10$ mV, as shown in Figure 6(b). This means that the electrophoretic velocity, $\vec{v}_{EP}$, and the electric field now point in opposite directions. Hence, according to our model, the ratio $\vec{v}_{DEP}/\vec{v}_{EK}$ increases when ζ_p takes on negative values. Furthermore, since in our experiments RNase A was suspended in a slightly basic buffer (pH = 8), the selection of a negative ζ_p value is supported by previous reports.[26] Note that when EP is excluded ($\zeta_p = 0$), the EK velocity is still higher (by $\sim$3 times) in comparison to the EK velocity response with $\zeta_p = -10$ mV (Figure 6(c)). A lower EK velocity is expected to reduce the drag force on the protein molecules, contributing to improve the dielectrophoretic trapping. In conclusion, pH plays an important role on the performance of dielectrophoretic traps as indicated by the simulated data presented in Figure 6. The dependency of protein electrokinetic transport on pH has already been experimentally, but not theoretically, demonstrated.[32] It should be noted that, since $\zeta_p = -10$ mV favored dielectrophoretic trapping (according to this parametric study), all the models presented herewith were solved taking into account such value for ζ_p.

IV. CONCLUSIONS

In this work, we have studied the electrokinetic phenomena involved in the transport of the mono-PEGylated RNase A and its native form within a microfluidic device. Herein, the electrokinetic transport mechanism was analyzed through a sphere model for the native RNase A and an ellipsoid model for the mono-PEGylated RNase A conjugate. Predictions of electrokinetic

phenomena obtained via 3D modelling using the COMSOL Multiphysics software were in agreement with the experimental observations as they were able to depict the streaming and trapping of the proteins at different applied electric potentials. Moreover, the model is allowed to calculate the magnitude and direction of the electrophoretic, electroosmotic, and dielectrophoretic velocities, providing more quantitative data and relating particle behavior to diverse parameters, e.g., electric potential, time period of electrical stimulus, and zeta-potential. Additionally, the study revealed that temperature increased significantly under trapping conditions inside the microfluidic channel. Although high temperatures may affect the biological activity of some proteins, RNase A can be stable up to 100 °C, and its mono-PEGylated specie can be even more stable due to the polymeric chain grafted to it. Nonetheless, evaluation of the enzyme activity of PEGylated RNase A should be further addressed experimentally after being subjected to high electric stimulus to estimate how much of the initial biological activity is retained. Also, the heat generated inside the microfluidic channel influenced the mechanic and electric properties of the medium, affecting the protein capture capabilities of the device. On the other hand, simulations demonstrated that the EK velocity can be reduced when the zeta potential takes on negative values, which is in agreement with experimental observations readily available in the literature.

We believe that the model presented in this work will allow the prediction of the electrokinetic response of different proteins in a microfluidic system. Therefore, the model itself can be a tool used to improve the design of microfluidic channels employed to separate and recover PEGylated proteins in one single step. Furthermore, the model can also aid in the development of heat control strategies inside electrokinetically driven microfluidic channels. Such strategies will allow the manipulation (i.e., separation, isolation, and concentration) of a wide range of proteins suspended in high electric conductivity solutions using high voltages without hindering their biological activity. In addition, this study has allowed understanding the impact of zeta potential, as a function of pH, on the dielectrophoretic trapping of proteins. Further studies must deal with the development of more robust mathematical models that are able to predict the gradient of H^+ ions inside the microfluidic channel when an electric stimulus is applied, calculate ζ_p as a function of pH, and consider the effect of Brownian motion on DEP-based protein manipulation dynamics. We consider that, by taking such phenomena into the model, it will be possible to enhance its estimation accuracy and therefore will lead to even decreasing correction factors.

ACKNOWLEDGMENTS

The authors would like to acknowledge the technological support of the FEMSA-Biotechnology Center as well as the financial support of the Biotechnology and Synthetic Biology Focus Group (Nos. 0820000100 and 0020DII001), and the Sensors and Devices Focus Group (No. 002EICII01). M.A.M.G. wishes to thank the National Council on Science and Technology of Mexico (CONACyT) for the Fellowship No. 204152.

[1]P. A. Leland and R. T. Raines, Chem. Biol. **8**, 405 (2001).
[2]J. Matoušek, P. Poučková, J. Souček, and J. Škvor, J. Controlled Release **82**, 29 (2002).
[3]G. Pasut and F. M. Veronese, Adv. Drug Delivery Rev. **61**, 1177 (2009).
[4]H. Tian, Y. Guo, X. Gao, and W. Yao, J. Pharm. Pharmacol. **65**, 53 (2013).
[5]J. A. Rodríguez-Martínez, I. Rivera-Rivera, R. J. Solá, and K. Griebenow, Biotechnol. Lett. **31**, 883 (2009).
[6]T. Z. Jubery, S. K. Srivastava, and P. Dutta, Electrophoresis **35**, 691 (2014).
[7]J. González-Valdez, L. F. Cueto, J. Benavides, and M. Rito-Palomares, J. Chem. Technol. Biotechnol. **86**, 26 (2011).
[8]K. Mayolo-Deloisa, J. González-Valdez, D. Guajardo-Flores, O. Aguilar, J. Benavides, and M. Rito-Palomares, J. Chem. Technol. Biotechnol. **86**, 18 (2011).
[9]R. C. Gallo-Villanueva, C. E. Rodríguez-López, R. I. Díaz-de-la-Garza, C. Reyes-Betanzo, and B. H. Lapizco-Encinas, Electrophoresis **30**, 4195 (2009).
[10]M. A. Saucedo-Espinosa and B. H. Lapizco-Encinas, Electrophoresis **36**, 1086 (2015).
[11]R. C. Gallo-Villanueva, N. M. Jesús-Pérez, J. I. Martínez-López, A. Pacheco, and B. H. Lapizco-Encinas, Microfluid. Nanofluid. **10**, 1305 (2011).
[12]F. Olasagasti and J. C. Ruiz de Gordoa, Transl. Res. **160**, 332 (2012).
[13]J. González-Valdez, M. Rito-Palomares, and J. Benavides, Anal. Bioanal. Chem. **403**, 2225 (2012).
[14]H. A. Pohl, J. Appl. Phys. **22**, 869 (1951).

[15]M. A. Mata-Gómez, R. C. Gallo-Villanueva, J. González-Valdez, S. O. Martínez-Chapa, and M. Rito-Palomares, Electrophoresis **37**, 519 (2016).
[16]M. Kahse, M. Werner, S. Zhao, M. Hartmann, G. Buntkowsky, and R. Winter, J. Phys. Chem. C **118**, 21523 (2014).
[17]G. H. Markx, P. A. Dyda, and R. Pethig, J. Biotechnol. **51**, 175 (1996).
[18]B. J. Kirby, *Micro- and Nanoscale Fluid Mechanics: Transport in Microfluidic Devices* (Cambridge University Press, New York, 2010).
[19]S. M. Daly, T. M. Przybycien, and R. D. Tilton, Biotechnol. Bioeng. **90**, 856 (2005).
[20]S. S. Pai, B. Hammouda, K. Hong, D. C. Pozzo, T. M. Przybycien, and R. D. Tilton, Bioconjugate Chem. **22**, 2317 (2011).
[21]R. W. Clarke, J. D. Piper, L. Ying, and D. Klenerman, Phys. Rev. Lett. **98**, 198102 (2007).
[22]A. Nakano, T.-C. Chao, F. Camacho-Alanis, and A. Ros, Electrophoresis **32**, 2314 (2011).
[23]J. I. Martínez-López, H. Moncada-Hernández, J. L. Baylon-Cardiel, S. O. Martínez-Chapa, M. Rito-Palomares, and B. H. Lapizco-Encinas, Anal. Bioanal. Chem. **394**, 293 (2009).
[24]I. Ermolina and H. Morgan, J. Colloid Interface Sci. **285**, 419 (2005).
[25]M. Wolf, R. Gulich, P. Lunkenheimer, and A. Loidl, Biochim. Biophys. Acta **1824**, 723 (2012).
[26]B. Krasniqi and J. S. Lee, PLoS One **9**, e88004 (2014).
[27]A. LaLonde, A. Gencoglu, M. F. Romero-Creel, K. S. Koppula, and B. H. Lapizco-Encinas, J. Chromatogr. A **1344**, 99 (2014).
[28]N. S. K. Gunda and S. K. Mitra, Biomicrofluidics **4**, 014105 (2010).
[29]C. F. Ivory and S. K. Srivastava, Electrophoresis **32**, 2323 (2011).
[30]B. H. Lapizco-Encinas, S. Ozuna-Chacón, and M. Rito-Palomares, J. Chromatogr. A **1206**, 45 (2008).
[31]K. Mayolo-Deloisa, M. E. Lienqueo, B. Andrews, M. Rito-Palomares, and J. A. Asenjo, J. Chromatogr. A **1242**, 11 (2012).
[32]A. Nakano, F. Camacho-Alanis, T.-C. Chao, and A. Ros, Biomicrofluidics **6**, 034108 (2012).
[33]R. C. Gallo-Villanueva, V. H. Pérez-González, R. V. Davalos, and B. H. Lapizco-Encinas, Electrophoresis **32**, 2456 (2011).
[34]H. Moncada-Hernandez, J. L. Baylon-Cardiel, V. H. Pérez-González, and B. H. Lapizco-Encinas, Electrophoresis **32**, 2502 (2011).
[35]R. C. Gallo-Villanueva, M. B. Sano, B. H. Lapizco-Encinas, and R. V. Davalos, Electrophoresis **35**, 352 (2014).
[36]A. Nakano, F. Camacho-Alanis, and A. Ros, Analyst **140**, 860 (2015).
[37]A. Gencoglu, F. Camacho-Alanis, V. T. Nguyen, A. Nakano, A. Ros, and A. R. Minerick, Electrophoresis **32**, 2436 (2011).
[38]H. Morgan and N. G. Green, *AC Electrokinetics: Colloids and Nanoparticles* (Research Studies Press, Hertfordshire, 2003).
[39]A. Nakano, J. Luo, and A. Ros, Anal. Chem. **86**, 6516 (2014).
[40]P. Lee, J. Towslee, J. Maia, and J. Pokorski, Macromol. Biosci. **15**, 1332 (2015).
[41]S. Salgın, U. Salgın, and S. Bahadır, Int. J. Electrochem. Sci. **7**, 12404 (2012).